

CFD simulation of blast in an internal geometry using a cartesian cell code

J. Tang¹

¹Department of Mechanical Engineering
University of Queensland, Brisbane, Queensland, 4072 AUSTRALIA

Abstract

CFD simulation of an explosion in an internal geometry representing a shipping container with venting is performed using an adaptive virtual cell embedding cartesian cell code. Virtual cell embedding is a simple method to approximate surfaces intersecting cells, allowing simple solution of the Euler equations in very complex geometries. The analysis is performed to produce contour maps of peak quantities like overpressure and impulse on the interior walls, and to ascertain the degree of amplification caused by shock focussing and reflection following movement of the blast wave along the geometry. Examples of the cartesian cell code being used to model flows in other geometries are also presented.

Introduction

The Centre for Hypersonics in the University of Queensland has recently considered the possibility of testing rocket motors in a confined facility (for purposes of safety and noise reduction). The facility in this case had the geometry of a modified shipping container with vents for the inlet and outlet. This paper presents a simplified numerical simulation of the worst-case scenario when the mainly nondetonable rocket propellant explodes in the facility. Attention will be paid to the magnitude of the peak impulse and overpressures generated on the (assumed rigid) internal walls. Due to the complex flowfield arising from both venting effects, shock focussing and shock reflection within the structure, a CFD code for modelling flows in complex geometries has been developed for use in this simulation.

Two approaches for modelling flows in complex geometry are by using unstructured grid [15] or cartesian cell methods [1]. Cartesian meshes treat solid objects as immersed within the grid and accord special treatment to intersected cells to account for the presence of a surface e.g. by adding extra surface flux terms. They offer some advantages over the more popular unstructured grids in terms of simplicity and regularity of implementation, efficiency, and accuracy [2, 8].

The code implements the virtual cell embedding (VCE) method [7, 6] as its cartesian cell method. It is a particularly simple method that subdivides intersected cells into discrete subcells to obtain the approximate obstructed cell areas and volumes, and can be used to make a fast calculation method for the Euler equations in complex geometries. The code solves a finite-volume formulation of these equations using a standard explicit (second order Runge-Kutta) MUSCL scheme. Also implemented is an octree h -refinement capability which increases efficiency by adding/deleting cells based on solution gradients. This paper will also present some code validation cases of transient, compressible flow in other geometries to demonstrate the usefulness of the numerical methodology.

The Virtual Cell Embedding (VCE) Method

The virtual cell embedding (VCE) method [7, 6] is a simple cartesian cell method that approximates the surface cutting through a cell as a single planar surface. The VCE method sub-

divides an intersected cell into a lattice of subcells each of which undergo point-inclusion tests with a body (figure 1). In this manner a summation of subcell volumes inside or outside bodies will yield the approximate obstructed and unobstructed cell volume respectively. Each cell face likewise undergoes subdivision to determine the approximate obstructed and unobstructed cell face area.

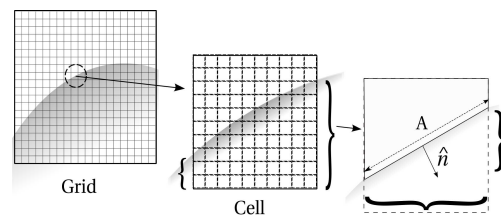


Figure 1: VCE illustration

This information is used to calculate the area and normal of the surface by approximating it as a single planar wall. Because of this single-plane approximation, VCE works best when the surface is not rapidly varying within a cell (which is most often the case). Convergence with VCE was demonstrated in simple planar and axisymmetric geometries [6, 14].

Code Validation

The code has been validated against previous numerical simulations and experimental data to demonstrate the effectiveness of the VCE method. Below are some examples of simulations of compressible, unsteady flow in various geometries that have been performed.

Shock-Cylinder Interaction

This two-dimensional example is of a mach 2.81 shock in air interacting with a cylinder. It is an interesting test case to observe how well VCE can represent curved surfaces. This problem has been investigated in the past using both finite difference and finite volume approaches [16, 18]. It has also been solved using Quirk's cartesian cell scheme [8], making it a good validation test case for the current cartesian cell scheme. The grid resolution used was similar to Quirk's [8] in order to resolve the vortex.

Figure 2 compares the computed density contours (top figure) with Quirk's solution (bottom figure). The comparison is generally favourable, with the shock, contact discontinuity, vortex and vortex stem all resolved quite well. The corresponding adapted grid can be seen in figure 3 which shows refinement at key flow features.

Pressure histories at various locations along the cylinder surface are plotted in figures 4 to 6. The time is normalized by the shock arrival time at the cylinder. These show the general good agreement between the computed results and results of Yang and Zoltak *et al* [16, 18].

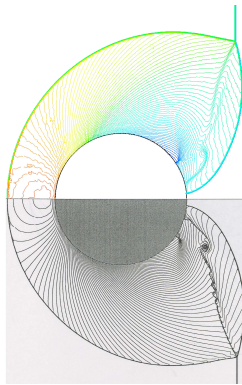


Figure 2: Comparison of density contours (top figure) for shock over a cylinder with the solution of Quirk [8] (bottom picture)

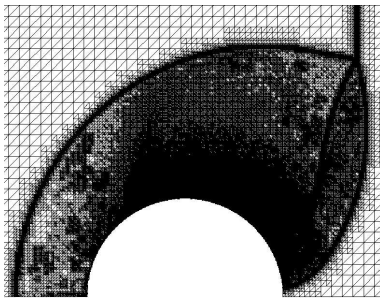


Figure 3: Adapted grid for shock over a cylinder

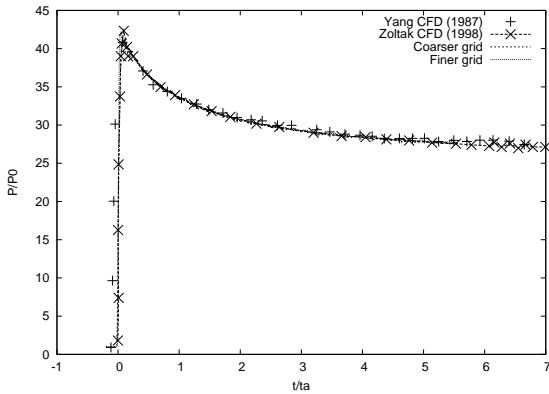


Figure 4: Pressure history at a point along cylinder (0°)

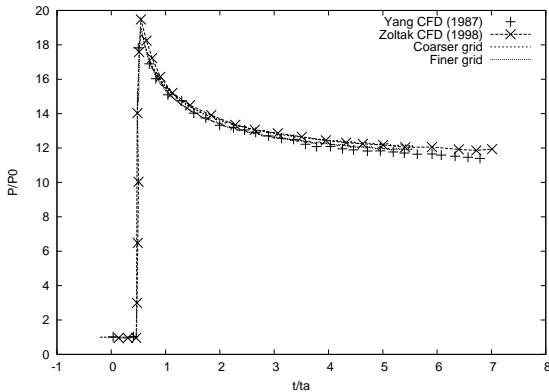


Figure 5: Pressure history at a point along cylinder (60°)

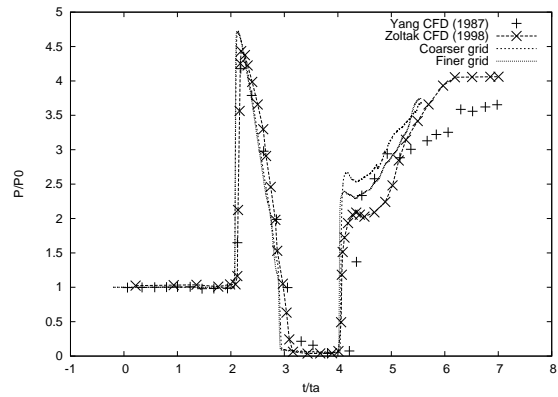


Figure 6: Pressure history at a point along cylinder (150°)

Blast in Cityscape

This three-dimensional example attempts to reproduce the simulation by Rose *et al* [3, 11] of an explosion in a complex cityscape environment. An experimental study was also performed to validate their results. Their simulation also used an adaptive cartesian cell code with similar numerical methodology and a polygon clipping algorithm to calculate cut cell data [10]. In the current simulation the same domain and cell size was chosen to achieve exactly correspondence in results. However, the explosive source was modelled by a group of high pressure and temperature cells with adjusted initial conditions to give proper blast energy.

Figure 7 shows the geometry and density contours on two planes some time after the explosion. Figures 8 to 10 plots pressure histories at some different locations within the domain and compares them with Rose's CFD and experimental results. Three different mesh refinement levels (corresponding to the grid refinement study in the original reference) were used to demonstrate convergence of results.

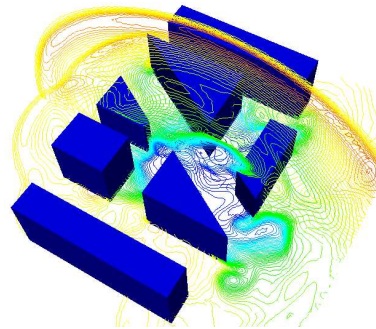


Figure 7: Density contours for explosion in cityscape problem

Agreement with Rose's results is generally quite good, although the computed waveforms are more diffuse. This is probably the result of different implementations of the explosive initial condition. Rose's code implements a multidimensional remapping procedure to resolve better the earlier stages of the blast wave.

Simulation of Explosion in Testing Facility

Rocket Motor Testing Facility

The rocket motor testing facility considered was a modified shipping container with vents for the inlet and outlet (located on the roof). A diagram of the facility is shown in figure 11. The walls were modelled as smooth, flat surfaces. The explo-

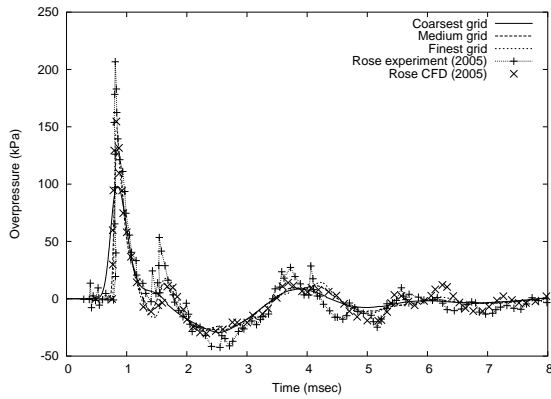


Figure 8: Pressure history at gauge 1 (at 0.6, 1.1, 0.105) of [11] for the explosion in cityscape problem

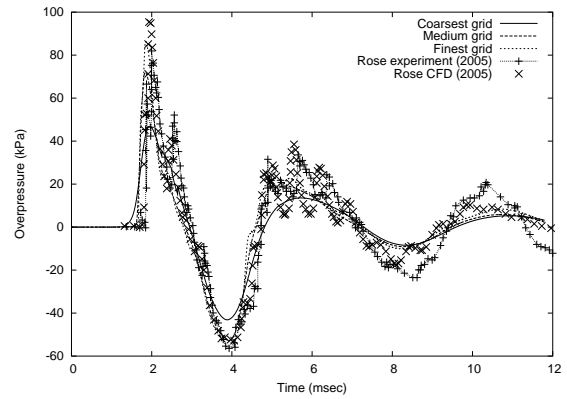


Figure 10: Pressure history at gauge 21 (at 1.56, 1, 0.075) of [11] for the explosion in cityscape problem

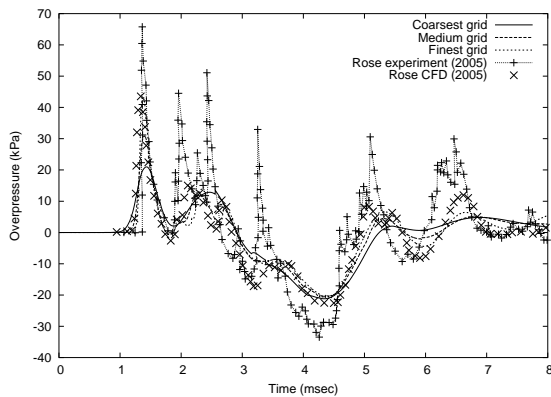


Figure 9: Pressure history at gauge 3 (at 0, 0.2, 0.075) of [11] for the explosion in cityscape problem

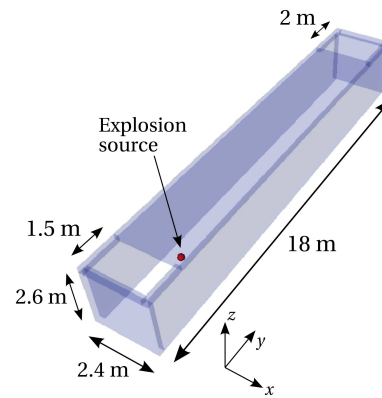


Figure 11: Diagram of testing facility

sive source is located along the container centerline, 3 m from the intake end and 1 m off the floor (this means a plane of symmetry along the centerline). The explosive energy from the predominantly ammonium perchlorate-based propellant was chosen to correspond to 20 kg of TNT, and was represented by a group of high pressure and temperature cells (an instantaneous detonation model).

Three minimum grid resolutions of roughly 0.23, 0.12 and 0.06 m cell sizes was used to investigate grid convergence. 225 trace points are distributed uniformly over each interior wall to obtain contours of peak quantities like overpressure P and impulse (the maximum value of $\int P dt$). The simulation was run to a sufficiently late time to ensure the primary blast wave has exited all vents. No fluid-structure interaction was modelled, with the walls modelled by rigid reflecting boundary conditions. Therefore the simulation models the explosion in can represent any rigid structure with the same internal geometry.

Convergence issues

It was found that the solutions from the three different meshes did not everywhere exhibit convergent behaviour. This can be seen in figure 12 where two pressure histories from different wall locations are plotted. The top figure shows good convergent behaviour in peak overpressure, whereas the bottom figure shows a larger difference between the two finest meshes than the two coarsest meshes.

A simulation was performed on a much finer grid (minimum cell size around 0.015 m) by reducing the domain size to only

encompass the inlet-end wall. Thus up until an early time (around 5 ms) solutions on the inlet-end wall between the larger and shorter domains could be compared. It was observed that the average error in impulse values between the larger and shorter domain grids was around 3% (quite good), but in peak overpressure was as much as 23%. Impulse, being the integral of pressure over time, is less sensitive to error and grid resolution than a single quantity like overpressure.

There are some reasons why convergent behaviour was difficult to achieve for this problem. (1) The problem's three-dimensional nature and relatively large computational domain limited the number of cells to ensure computation within acceptable memory and time limits, (2) the solution also depends to an extent on the initial explosive shape, which is varies with grid resolution. (3) The solution at farther distances depends on how well shock focussing and reflection is captured at earlier stages as the blast interacts with the facility interior, which is in turn quite dependent on cell resolution, and (4) the mesh was not always adapted to the finest level at surfaces due to the grid adaptation criterion implemented.

Although not all parts of the contour maps of peak quantities along the interior walls will display convergent behaviour, qualitative data can still be extracted. As peak pressures increase in value for increasingly finer meshes, these contours represent minimum bounds on the true solution.

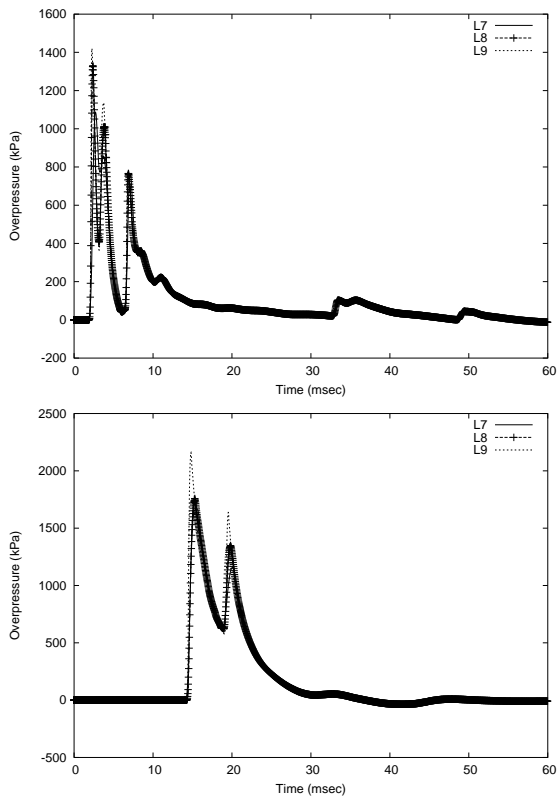


Figure 12: Some pressure histories for the explosion in internal geometry problem. The top picture shows convergent behaviour, the bottom does not.

Contour Map Results

The contour maps of peak overpressure and impulse along the facility's interior walls are shown in figures 13 to 16. These contours have been produced from the finest resolution mesh. Some brief comment on each figure is given below.

Figure 13 shows the peak quantities along the long side wall. Note that peak values occur at the charge location, and are greatest at corners at edges due to focussing. Peak pressures are of the order of tens of megapascals. It is interesting that the impulse is nearly constant along the wall section from the charge to the outlet vent.

Figure 14 plots contours along the inlet-end wall. It is interesting that there are two distinct maximum pressures that occur near but not exactly at the floor of the facility ($z = 0$). The impulse plot shows greater values along the floor edge, which is due to the shock focussing there and the charge height of burst.

Figure 15 shows contours along the outlet-end wall, which is farthest from the charge. By this stage the waveforms have undergone some numerical diffusion and thus the contours are smoothly varying. Peak pressure occurs at the facility floor and have attenuated to the order of megapascals. Impulse values are also greatest at the floor.

Figure 16 plots peak values along the interior ceiling. There exists a local maximum in pressure directly above the charge itself, although peak values occur at edges (at the charge location) due to focussing. The effect of venting on reducing peak values can be seen on the impulse plot where a marked decrease can be observed. The impulse is nearly constant along the section from the charge to the outlet vent.

Pressure Amplification and Failure on the Outlet Wall

It is interesting to see just how much larger the overpressures are at the far-end outlet wall and outlet vent compared to a free field air burst. The amplification arises from the blast wave travelling through a contained space with multiple shock focussing and reflection. It was found based on the trace data on the finest resolution mesh that the average peak overpressure on the outlet wall and outlet vent was 1.66 MPa and 0.5 MPa respectively. The peak overpressure at the vent corresponded to a reflected shock from the outlet wall (the initial incoming shock had a lower peak).

Using scaled spherical TNT free field data from Kinney [5], it was found that at the same scaled distance as the outlet wall the overpressure would be around 0.024 MPa. Assuming a shock with this overpressure undergoes normal reflection, the reflected overpressure can be calculated via the Rankine-Hugoniot relations to be 0.053 MPa. This means amplification factors at the outlet wall and vent of *at least* 31 and 9.4 respectively. Simpler (but faster) semiempirical methods [4, 12] for overpressure estimation based on design curves in free air burst would underestimate greatly the overpressures in this internal geometry even at farther distances from the charge. This conclusion is also repeated in previous experimental and numerical studies on the effect of blast channeling in street geometries [9, 13]

Approximating the outlet wall as a simply-supported flat plate of thickness 5 mm subject to the uniform load of 1.66 MPa, it is possible to calculate the maximum wall stress (located at the wall center) by a simple formula obtainable from a solid mechanics text [17]. As the wall is a nearly square section, the stress is simply $0.2874q(L/t)^2$ where q is the load, L and t are the length and thickness respectively. It was computed to be 110 GPa; this is clearly much higher than the tensile strength of the steel wall (which is on the order of hundreds of megapascals), making failure very likely (at least at the wall center).

If wall failure alone is being investigated, it is unnecessary to use numerical simulation, as hand calculation via Kinney's scaled data [5] would be sufficient to demonstrate this. As the reflected overpressure is calculated to be 0.053 MPa (based on Kinney's curve), the computed stress is 3.5 GPa, which is still too high. Failure on at least some parts of the other walls in closer proximity to the explosive source can probably be assumed. In reality the walls are corrugated, effectively raising stiffness, and are not simply supported at their edges. More detailed modelling of the wall response is best obtained via a finite element simulation.

Conclusion

An adaptive virtual cell embedding CFD code has been used to obtain compute contour maps of important quantities like peak overpressure and impulse along all walls of a rigid internal geometry subject to a blast from an explosive source. This scenario corresponds to a simplified model of a detonating rocket motor in a modified shipping container testing facility. The code has also been used effectively to model compressible, transient flows in other geometries. In this internal geometry, amplification of overpressure at the far-end outlet wall of the structure was shown to be much larger than that predicted via the free field TNT design curves. A grid refinement has shown that peak impulse values along the walls was computed quite reliably, although grid independence was not fully achieved for all simulations.

Acknowledgements

The author thanks Dr. Peter Jacobs, Dr. Philip Teakle and Dr

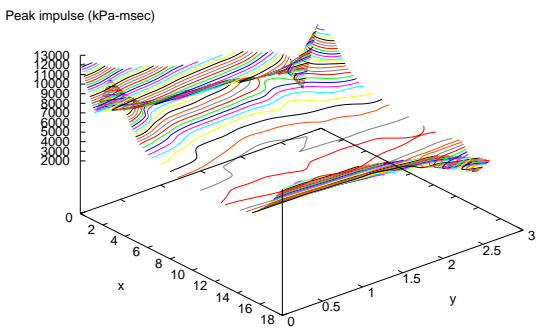
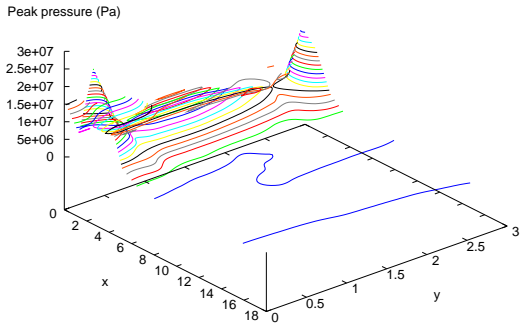


Figure 13: Contour maps for the long side wall. Top figure – pressure. Bottom figure – impulse

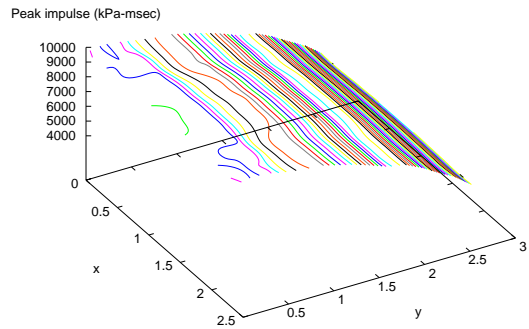
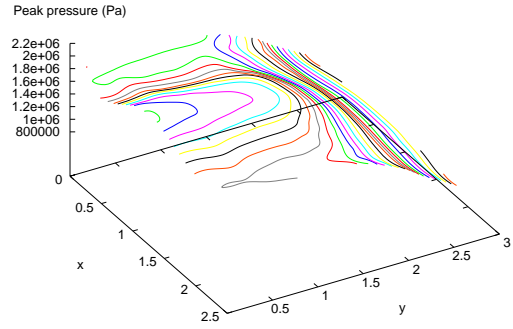


Figure 15: Contour maps for the outlet-end wall. Top figure – pressure. Bottom figure – impulse

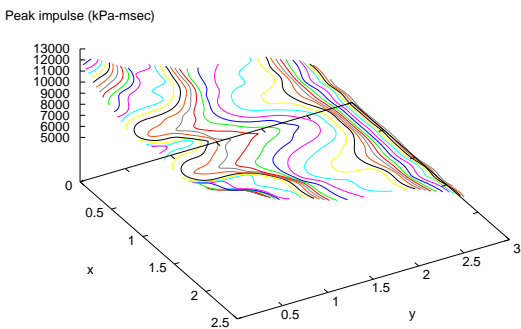
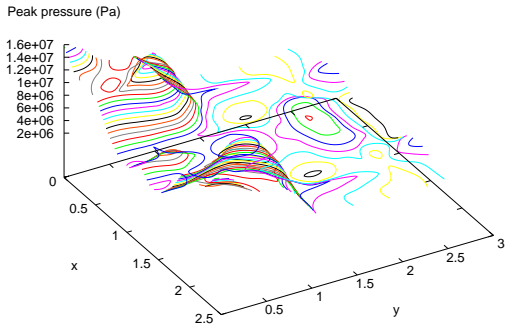


Figure 14: Contour maps for the inlet-end wall. Top figure – pressure. Bottom figure – impulse

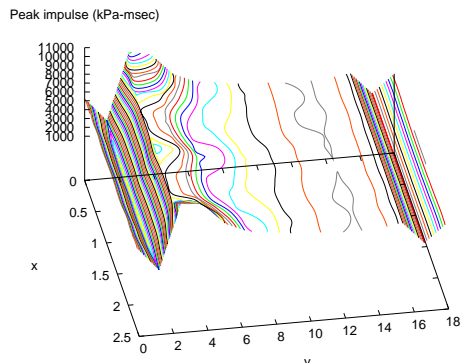
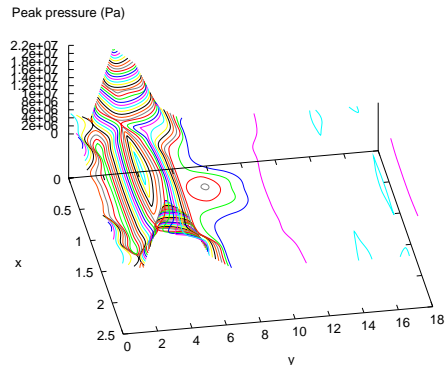


Figure 16: Contour maps for the ceiling wall. Top figure – pressure. Bottom figure – impulse

Charlotte Nash-Stewart for supplying detail on the facility geometry and explosion source characteristics.

References

- [1] Aftosmis, M. J., Solution adaptive cartesian grid methods for aerodynamics flows with complex geometries, 1997, 28th Computational Fluid Dynamics Lecture Series.
- [2] Berger, M. J. and LeVeque, R. J., An Adaptive Cartesian Mesh Algorithm for the Euler Equations in Arbitrary Geometries, 1989, aIAA 89–1930–CP.
- [3] Brittle, M. A., *Blast Propagation in a Geometrically Complex Urban Environment*, Master's thesis, Royal Military College of Science Engineering Systems Department, 2004.
- [4] Henrych, J., *The Dynamics of Explosion and Its Use*, Elsevier Scientific Publishing Company, Czechoslovakia, 1979.
- [5] Kinney, G. F., *Explosive Shocks in Air*, Springer-Verlag Berlin Heidelberg, 1985, 2nd edition.
- [6] Landsberg, A. M. and Boris, J. P., The Virtual Cell Embedding method: a simple approach for gridding complex geometries, 1997, aIAA–97–1982.
- [7] Landsberg, A. M., Boris, J. P., Young, T. R. and Scott, R. J., Computing Complex Shocked Flows Through the Euler Equations, in *Shock waves at Marseille: Proceedings of the 19th International Symposium on Shock Waves*, 1993, 421–426, 421–426.
- [8] Quirk, J. J., An alternative to unstructured grids for computing gas dynamic flows around arbitrarily complex two-dimensional bodies, *Computers Fluids*, **23**, 1994, 125–142.
- [9] Rose, T. A. and Smith, P. D., The influence of street junctions on blast wave impulses produced by vehicle bombs, in *Proceedings of the 11th International Symposium on Interaction of the Effects of Munitions with Structures, New Orleans, USA*, 2003.
- [10] Rose, T. A. and Smith, P. D., Development of an adaptive mesh CFD code for high explosive blast simulation, in *Proceedings of the 12th International Symposium on Interaction of the Effects of Munitions with Structures, New Orleans, USA*, 2005.
- [11] Rose, T. A., Smith, P. D. and Brittle, M., Analysis of a generic cityscape using an adaptive mesh CFD code, in *Proceedings of the 12th International Symposium on Interaction of the Effects of Munitions with Structures, New Orleans, USA*, 2005.
- [12] Smith, P. D. and Hetherington, J. G., *Blast and Ballistic Loading of Structures*, Butterworth and Heinemann Ltd., Oxford, 1994.
- [13] Smith, P. D., Whalen, G. P., Feng, L. J. and Rose, T. A., Blast loading on buildings from explosions in city streets, *Structures and Buildings*, **146**, 2001, 47–55.
- [14] Tang, J., A simple axisymmetric extension to Virtual Cell Embedding, 2007, submitted to the International Journal for Numerical Methods in Fluids.
- [15] Timofeev, E., Voinovich, P. and Takayama, K., Adaptive Unstructured Simulation of Three-Dimensional Blast waves with Ground Surface Effect, in *36th Aerospace Sciences Meeting and Exhibit*, 1998, aIAA 98–0544.
- [16] Yang, J. Y., Liu, Y. and Lomax, H., Computation of Shock Wave Reflection by Circular Cylinders, *AIAA Journal*, **25**, 1987, 683–689.
- [17] Young, W. C., *Roark's Formulas for Stress and Strain*, McGraw-Hill Book Company, USA, 1989, 6th edition.
- [18] Zóltak, J. and Drikakis, D., Hybrid upwind methods for the simulation of unsteady shock-wave diffraction over a cylinder, *Computer Methods in Applied Mechanics and Engineering*, **162**, 1998, 165–185.